# Heterobivalent Agents Targeting PSMA and Integrin-$\alpha_v\beta_3$

Hassan M. Shallal, Il Minn, Sangeeta R. Banerjee, Ala Lisok, Ronnie C. Mease, and Martin G. Pomper*

Russell H. Morgan Department of Radiology and Radiological Science, Johns Hopkins Medical Institutions, Baltimore, Maryland 21287, United States

S *Supporting Information*

ABSTRACT: Differential expression of surface proteins on normal vs malignant cells provides the rationale for the development of receptor-, antigen-, and transporter-based, cancer-selective imaging and therapeutic agents. However, tumors are heterogeneous, and do not always express what can be considered reliable, tumor-selective markers. That suggests development of more flexible targeting platforms that incorporate multiple moieties enabling concurrent targeting to a variety of putative markers. We report the synthesis, biochemical, *in vitro,* and preliminary *in vivo* evaluation of a new heterobivalent (HtBv) imaging agent targeting both the prostate-specific membrane antigen (PSMA) and integrin-$\alpha_v\beta_3$ surface markers, each of which can be overexpressed in certain tumor epithelium and/or neovasculature. The HtBv agent was functionalized with either 1,4,7,10-tetraazacyclododecane-1,4,7,10-tetraacetic acid (DOTA) or the commercially available IRDye800CW. DOTA-conjugated HtBv probe **9** bound to PSMA or $\alpha_v\beta_3$ with affinities similar to those of monovalent (Mnv) compounds designed to bind to their targets independently. *In situ* energy minimization experiments support a model describing the conformations adapted by **9** that enable it to bind both targets. IRDye800-conjugated HtBv probe **10** demonstrated target-specific binding to either PSMA or integrin-$\alpha_v\beta_3$ overexpressing xenografts. HtBv agents **9** and **10** may enable dual-targeted imaging of malignant cells and tissues in an effort to address heterogeneity that confounds many cancer-targeted imaging agents.
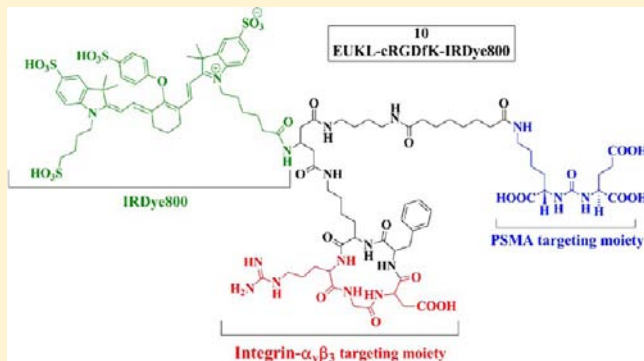
■ INTRODUCTION

Phenotypic differences between normal and malignant cells form the basis for cancer-selective targeting of imaging and therapeutic agents. Proteins overexpressed on the cell surface have received considerable attention in that regard because of their accessibility relative to intracellular targets, particularly for bulky and/or charged multimodality imaging and multifunctional therapeutic agents. Accordingly, this has resulted in developing various affinity agents including antibodies, antibody fragments, aptamers, peptides, and small molecules in addition to refining the mechanisms of their attachment to imaging agents, drugs, and nanoparticles.

Cancer cell surface proteins have been used extensively for diagnosis, staging, and therapeutic monitoring.[1,2] For example, patients with prostate cancer are beginning to benefit from targeted affinity agents for improved imaging of local and metastatic disease, and for detection and isolation of circulating tumor cells.[3−6] Those cancer-selective surface markers, including but not limited to the prostate-specific membrane antigen (PSMA), hepsin, chemokine receptors such as CXCR4, and integrin-$\alpha_v\beta_3$, are overexpressed in different stages and phenotypes of prostate cancer.[1,7] Here we focus on developing imaging agents that target two disparate surface targets, to enable imaging of tumor cells that might possess one but not the other. Recently, rational multitargeting strategies have emerged based on the hypothesis that simultaneous targeting of multiple sites

promises a greater overall therapeutic impact compared to targeting a single site.[8−11] The concept of targeting more than one cell surface protein for imaging purposes has been demonstrated by Gillies and coworkers using a heterobivalent (HtBv) agent that enables dual recognition of human melanocortin and cholecystokinin receptors both *in vitro* and *in vivo.*[12,13] Dual targeting of integrin-$\alpha_v\beta_3$ and gastrin releasing peptide receptor (GRPR) using several imaging modalities has also been demonstrated.[14−16] There are several advantages to multitargeting approaches. First, they can improve the sensitivity of detection through synergistic increase of binding affinities to targets. Second, the specificity of detection can be enhanced. Third, one can use a single agent to target multiple surface markers that are differentially expressed on cancer cells with progression of the disease.

PSMA is a type II transmembrane glycoprotein that is overexpressed in prostate cancer, particularly in metastatic and hormone-refractory disease.[17] Small molecules have been developed to target PSMA selectively for imaging with single photon emission computed tomography (SPECT), positron emission tomography (PET), and optical imaging[18−22] with several radionuclide-based agents proceeding to clinical trials.[4,5]

Table 1. ESI-MS and HPLC Data

compound	exact mass	found mass		mass spectrum	Analytical HPLC method	t_R (min)	HPLC chromatogram
		$(M + 1)^{+1}$	$(M + 2)^{+2}/2$				
2	545.31	546.7	-	Figure S2	1	14.9	Figure S3
3	931.49	931.9	466.5	Figure S4	2	10.52	Figure S5
4	603.31	604.4	-	Figure S6	2	11.19	Figure S7
5	989.49	989.8	495.4	Figure S8	2	12.03	Figure S9
6	1587.54	1587.3	794.3	Figure S10	5	9.1	Figure S11
7	440.4	463.9 $(M + Na)^{+1}$		Figure S12	4	16.18	Figure S13
8	1259.65	1260.7	630.8	Figure S14	2	16.29	Figure S15
9	1645.83	1645.7	823.5	Figure S16	3	10.78	Figure S17
10	2243.88	2243.6	1122.6	Figure S18	5	8.48	Figure S19

PSMA has been targeted to deliver therapeutic nanoparticles both in experimental models and in cancer patients.[23] In addition to prostate cancer, PSMA is overexpressed in tumor neovasculature, a property that can be leveraged for imaging a wide variety of tumors.[24−26]

Integrins, a family of transmembrane proteins, have been found to be dysregulated in several varieties of cancer as well as in other disorders such as inflammation and fibrosis. They are involved in a variety of activities that occur between cancer cells and their surrounding environment.[27,28] One target for imaging cancer is $\alpha_v\beta_3$ integrin, and we have employed a standard affinity agent to enable its imaging in this report. We have chosen this target in part because of its diverse functions related to tumor progression, and also because it is expressed in tumor neovasculature, as is PSMA.[29−31] As such, $\alpha_v\beta_3$ integrin provides a reasonable cotarget along with PSMA for tumor neovasculature. Notably, other functions of $\alpha_v\beta_3$ integrin include cancer cell migration and metastasis.[32] Because of these important roles in cancer, and its presence on tumor neovasculature, $\alpha_v\beta_3$ integrin has been a frequent target for the development of site-directed molecular imaging agents, many of which incorporate the Arg-Gly-Asp (RGD) binding motif.[33]

Here we describe a multitargeting strategy utilizing PSMA and $\alpha_v\beta_3$ integrin simultaneously. We synthesized a dual PSMA/$\alpha_v\beta_3$ integrin targeted imaging agent by incorporating a low-molecular-weight, urea-based PSMA inhibitor and a cyclic RGD (cRGDfK) peptide into the same construct. The HtBv probe was then conjugated to 1,4,7,10-tetraazacyclododecane-1,4,7,10-tetraacetic acid (DOTA) or to a commercially available near-infrared light-emitting dye (IRDye800CW) to enable its ultimate use for imaging and/or radiometal therapy. The binding of the DOTA-conjugated derivative was compared to the corresponding monomeric DOTA-conjugated compounds using several biochemical assays against both surface proteins. In addition we used *in situ* ligand minimization in an attempt to predict the mode of binding of the DOTA-conjugated HtBv agent **9** to its protein targets. Lastly, we used the IRDye800-conjugated agent **10** for optical imaging of either PSMA or $\alpha_v\beta_3$ overexpressing xenografts by observing its target-specific, dose-dependent uptake.

■ EXPERIMENTAL PROCEDURES

Chemistry. All commercial starting materials were used without further purification. Protected amino acids were purchased from ChemImplex (Wood Dale, IL), DOTA-NHS ester was obtained from Macrocyclics (Dallas, TX), IRDye800CW-YC27 and IRDye-800CW NHS ester were obtained from LI-COR (Lincoln, NE), and glycine loaded 2-chlorotrityl-chloride resin (0.51 mmol/g, 100−200 mesh) was obtained from AAPPTec (Louisville, KY). All other reagents were purchased from Sigma-Aldrich (Milwaukee, WI). Reaction products were purified using semipreparative high-performance liquid chromatography (HPLC) followed by structural elucidation using NMR and/or ESI-MS. A Bruker UltraShield 400 MHz spectrometer was used to obtain ^{1}H NMR and ^{13}C NMR spectra. Chemical shifts (δ) are reported in ppm downfield from proton resonance resulting from incomplete deuteration of CDCl$_3$, which was used as the NMR solvent. Low resolution ESI-MS spectra were obtained using a Bruker Daltonics Esquire 3000 Plus spectrometer (Fremont, CA). ESI-MS characterization is described for all newly synthesized intermediates and final compounds in Table 1. Semipreparative HPLC purification was performed utilizing a Waters 600E Delta LC system with a Waters 486 variable wavelength UV/vis detector, both controlled by Waters Empower software (Milford, MA), and a semi-preparative Phenomenex column [5 μ, C18(2), and 250 × 10 mm] (Torrance, CA). Solvent-A was 0.1% TFA in water whereas solvent-B was 0.1% TFA in acetonitrile. Purification required a compound-optimized gradient with flow rate of 4 mL/min and detection at 220 and 254 nm. The purity of the isolated key intermediates and the final compounds was further confirmed using the same HPLC conditions. Several elution gradient methods were developed: Method-1: from 95% to 75% solvent-A over 20 min; Method-2: from 90% to 70% solvent-A over 20 min; and Method-3: from 85% to 55% solvent-A over 30 min. Method-4 was run from 70% to 50% solvent-A over 20 min, employing detection at 210 and 220 nm. For compounds conjugated to IRDye800, Method-5 was developed with an isocratic elution of 80% solvent-A for 2.5 min followed by a gradient to 60% solvent-A over 10 extra min and to 80% solvent-A for 2.5 min with a flow rate of 6 mL/min and detection at 220 and 700 nm. Analytical HPLC characterization (t_R) is given in Table 1 for all synthesized intermediates and final compounds. In the case of IRDye800 conjugates, the quantity obtained was determined using a standard calibration curve of the relationship between concentration and absorbance at both 700 and 750 nm. The calibration curve was constructed by measuring the absorbance of serial dilutions of the IRDye800-NHS ester at both 700 and 750 nm using a ND1000 spectrophotometer (Wilmington, DE) (Figure S1). Peptide synthesis was executed using a CEM Liberty microwave peptide synthesizer (Matthews, NC) and PepDriver software.

Synthesis of EUKL-NH$_2$ (2). The amine-terminated intermediate **2** was obtained from the corresponding protected NHS ester **1**, which was synthesized as previously reported.[34] Compound **1** (74 mg, 100 μmol) was reacted with *N*-boc-1,4-diaminobutane (19 mg, 100 μmol) and TEA (20 μL) in CH$_2$Cl$_2$ (2 mL). The reaction was monitored using ESI-MS and

evaporated under vacuum upon completion. The crude product was deprotected by stirring in 1:1 TFA/CH_2Cl_2 (2 mL) at ambient temperature for 2 h. The final product was obtained by evaporation under vacuum followed by semipreparative HPLC (Method-1) affording 25 mg (45 μmol, yield = 46%).

Synthesis of EUKL-DOTA (3). Intermediate **2** (8 mg, 14 μmol) was dissolved in 300 μL DMF to which 30 μL diisoproylethyl-amine (DIPEA) was added. To the aforementioned solution, DOTA-NHS ester (10 mg, 14 μmol) was added. The reactants were mixed thoroughly and kept at ambient temperature for 2 h. The conjugation reaction was monitored using ESI-MS. Compound **3** was purified using HPLC (Method-2), which, following lyophilization, afforded 5 mg (5.3 μmol, yield = 38%).

Synthesis of cRGDfK-NH$_2$ (4). Intermediate **4** was synthesized using microwave assisted solid phase peptide synthesis (SPPS) following a published procedure, starting with 0.49 g of glycine-loaded 2-chlorotritylchloride resin (255 μmol).[35] The fully protected, open peptide was cyclized using diphenylphosphor-ylazide (DPPA) and NaHCO$_3$.[36] A mixture of the crude protected acyclic peptide (1 equiv, 90 μmol, 100 mg), NaHCO$_3$ (5 equiv, 450 μmol, 36 mg), DMF (100 mL), and DPPA (3 equiv, 270 μmol, 80 mg) was stirred overnight. Upon confirming the completion of cyclization by ESI-MS, the solvent was evaporated under vacuum and deprotection was performed without purification using a mixture of TFA, H$_2$O, and TES (95:2.5:2.5). The reaction mixture was concentrated under vacuum and the final product was purified using HPLC (Method-2) generating 36 mg of pure peptide (60 μmol, overall yield = 24%).

Synthesis of cRGDfK-DOTA (5). Intermediate **4** (4.2 mg, 7 μmol) was conjugated with DOTA-NHS ester (6.4 mg, 8 μmol) using a conjugation procedure similar to that for **3**. Compound **5** was obtained after HPLC purification using Method-2 (5.5 mg, 5.5 μmol, yield = 79%).

Synthesis of cRGDfK-IRDye800 (6). Intermediate **4** (0.5 mg, 0.8 μmol) was conjugated with 0.5 mg IRDye800CW NHS ester (0.4 μmol) in a mixture of 100 μL DMSO and 5 μL DIPEA. Reactants were mixed thoroughly for 2 h at ambient temperature. The conjugated derivative **6** was purified using HPLC (Method-5) to yield 200 nmol (yield = 50%), quantified using a standard calibration curve (Figure S1).

Synthesis of Bis(2,5-dioxopyrrolidin-1-yl) 3-((tert-butoxycarbonyl)amino)pentanedioate (7). Boc-protected β-glutamic acid was prepared from β-glutamic acid following a previously reported procedure.[37] The crude boc-protected β-glutamic acid (400 mg, 1.62 mmol) was dissolved along with *N*-hydroxysuccinimide (NHS, 2.2 equiv, 409 mg, 3.56 mmol) in 6 mL anhydrous DMF. To this mixture, 3-(ethyliminomethyle-neamino)-*N*,*N*-dimethylpropan-1-amine hydrochloride (EDAC.HCl, 2.2 equiv, 684 mg, 3.56 mmol) was added and the reaction was stirred for 48 h at ambient temperature. The solvent was then evaporated under vacuum, 0.1 N HCl was added to the residue, and extraction using ethyl acetate was performed (3×). Organic fractions were combined, washed with water, NaHCO$_3$, NaCl; dried using anhydrous Na$_2$SO$_4$; and concentrated under vacuum. The residue obtained was purified by HPLC (Method-4) to yield a white solid (100 mg, yield = 15%). ^{1}H NMR (CDCl$_3$): δ-4.51 (m, 1H, CHNH boc), 3.05 (m, 4H COCH$_2$), 2.83 (s, 8H, succinimide), and 1.437 (s, 9H, t-butyl). ^{13}C NMR (CDCl$_3$): δ 168.83 (4C, succinimide carbonyl groups), 166.04 (2C, OCO), 154.78 (1C, NHCOO), 80.25 (1C, OCH), 44.35 (1C, NHCH), 34.87 (2C, COCH2), 28.29 (3C, CH3), 25.59 (4C, succinimide methylene groups, CH$_2$CH$_2$).

Synthesis of EUKL-cRGDfK-NH$_2$ (8). To a solution of **7** (3.5 mg, 8 μmol) in 250 μL DMF and 25 μL DIPEA, a solution of **2** (5 mg, 9 μmol) and **4** (5.5 mg, 9 μmol) in 250 μL DMF was added. The reaction mixture was left for 2 h at ambient temperature and then concentrated under vacuum. The boc-protected inter-mediate was deprotected *in situ* without purification using 500 μL of a mixture of TFA, H$_2$O, and tetraethylsilane (TES) (95:2.5:2.5). The reaction mixture was concentrated and the final intermediate **8** was purified using semipreparative HPLC (Method-2) affording 5 mg (4 μmol, yield = 50%).

Synthesis of EUKL-cRGDfK-DOTA (9). The DOTA-con-jugated HtBv agent **9** was synthesized *via* the conjugation of intermediate **8** (2 mg, 1.5 μmol) and DOTA-NHS ester (1.4 mg, 1.8 μmol) according to the procedure described for **3**. The reaction mixture was concentrated and the target compound was purified using HPLC (Method-3) providing 2 mg (1.2 μmol, yield = 80%).

Synthesis of EUKL-cRGDfK-IRDye800 (10). The IRDye800-conjugated HtBv agent **10** was synthesized *via* the conjugation of intermediate **8** (1 mg, 0.7 μmol) and IRDye800CW NHS ester (0.5 mg, 0.4 μmol) in 100 μL DMSO and 5 μL DIPEA. After 2 h at ambient temperature, the conjugated derivative **10** was purified using HPLC (Method-5) to yield 40 nmol (yield = 10%), quantified using a standard calibration curve of the dye (Figure S1).

NIR Cell-Based Binding Assays. PSMA-positive (PC-3/PIP) and PSMA-negative (PC-3/flu) sublines were generously provided by Dr. Warren Heston (Cleveland Clinic). Both cell lines were grown in F-12K medium (Mediatech Inc., Manassas, VA) containing 10% FBS (Sigma Aldrich, St. Louis, MO) and Pen-Strep (Mediatech Inc., Manassas, VA). Human glioblastoma U87-MG cells, reported to express $\alpha_v\beta_3$ integrin,[38] generously provided by Dr. John Laterra (Johns Hopkins University), were grown in MEM medium (Mediatech Inc., Manassas, VA) supplemented with 10% FBS and Pen-Strep. All cell cultures were maintained at 5% carbon dioxide (CO$_2$) at 37 °C in a humidified incubator. All cell-based experiments were performed using the Nunc Edge 96-well plates (Fischer Scientific, Pittsburgh, PA) in order to prevent differential evaporation rates from the inside to the outside wells, which cause variation in the rate of cell growth between the peripheral and the internal wells of the plate. PSMA+ PC-3/PIP and PSMA- PC-3/flu cells were seeded at a density of 2 × 10^4 cells per well and incubated for 24 h prior to the binding experiment (binding isotherm or competitive binding). Binding experiments to PC-3 cells were conducted in the same media used to support their growth. After adding the indicated amount of compound, cells were incubated in 5% CO$_2$ at 37 °C in a humidified incubator for 30 min. Cells were washed twice using serum-free media followed by reading the near-infrared (NIR) optical signal of the entire plate using Odyssey NIR imaging system version 3.0 (LI-COR, Lincoln, NE). About 8 × 10^4 U87-MG cells were plated per well on the same 96-well plate and incubated for 48 h prior to the binding experiment. In contrast to the conditions adopted for binding to PC-3 cells, binding experiments for U87-MG cells were conducted in binding buffer (50 mM Tris, pH 7.4, 100 mM NaCl, 2 mM CaCl$_2$, 1 mM MgCl$_2$, 1 mM MnCl$_2$, and 1% bovine serum albumin) for 2 h at 25 °C prior to washing twice using cold binding buffer followed by reading the NIR signal of the entire plate.[39] The DOTA-conjugated compounds were allowed to compete against a fixed concentration of an NIR-emitting agent. In the case of targeting PSMA expressed on the surface of PC-3/PIP cells, IRDye800-YC27 was used (Figure S20).[21] For

targeting $\alpha_v\beta_3$ integrin expressed on the surface of U87-MG cells, **6** was used. The NIR signal was recorded using the LI-COR Odyssey NIR imaging system version 3.0, preset using the microplate option and with the following parameters assigned during measurement: resolution = 169 μm, medium quality, focus offset = 3 mm, intensity = 800, channel = 7. All measurements were performed in quadruplicate.

Binding Isotherms. In order to determine the dissociation constant (K_d) of a NIR agent with respect to binding to its target cells, a binding isotherm was constructed by measuring the uptake of serially diluted solutions of the agent against a fixed number of cells. The binding isotherms of IRDye800-YC27 to PC-3/PIP (test binding), PC-3/flu (biological nonspecific binding), and the plate (physical nonspecific binding) were recorded. Similarly, the binding isotherm of **6** to U87-MG cells was recorded. Binding isotherms were constructed by plotting the concentration of the agent (nM) against the measured integrated fluorescence intensity. The binding isotherms were fitted using nonlinear regression with a one site binding module available in GraphPad Prism version 4.00 for Windows (GraphPad Software, San Diego, CA).

Z-Factor Calculations. Two plates were used to measure the maximum signal produced by the binding of 10 nM IRDye800-YC27 to 3×10^4 PC-3/PIP cells/well, whereas two plates were used to measure the minimum signal resulting from blocking the binding of 10 nM IRDye800-YC27 by 10 μM of 2-[3-[1-carboxy-5-(4-iodobenzoylamino)-pentyl]-ureido]-pentanedioic acid (DCIBzL) as a high-affinity PSMA binding agent.[20] The readings were processed using the following equation in order to compute the Z-factor:[40]

$$Z = \frac{|\mu_{C+} - \mu_{C-}| - |3\sigma_{C+} - 3\sigma_{C-}|}{|\mu_{C+} - \mu_{C-}|} = 1 - \frac{|3\sigma_{C+} - 3\sigma_{C-}|}{|\mu_{C+} - \mu_{C-}|}$$

where μ_{C+} is the mean of the maximum signal and μ_{C-} is the mean of the minimum signal, ρ_{C+} is the standard deviation of the maximum signal, and ρ_{C-} is the standard deviation of the minimum signal.

Competitive Binding Inhibition. The Mnv and HtBv compounds were tested for their ability to displace the corresponding NIR agent from the respective protein target expressed on the cell surface. Serial dilutions of 10 000, 1000, 100, 10, 1, 0.1, 0.01, and 0 nM of each test compound were prepared. One experiment was executed against 10 nM of IRDye800YC27 using PC-3/PIP cells whereas the other was performed using 50 nM of cRGDfK-IRDye800 (**6**) and U87-MG cells. The competitive binding curves were fitted using nonlinear regression analysis and IC_{50} values were assigned when 50% of the corresponding agent was displaced.

PSMA Binding Assay. To compare the PSMA functional inhibition of **9** to its Mnv analog **3** and a positive control (DCIBzL), a fluorescence-based glutamate-hydrolysis inhibition assay was implemented according to a published procedure (Amplex red assay).[20] All dilutions were performed in quadruplicate. The binding curves were fitted as described above.

$\alpha_v\beta_3$ *Integrin Binding Assay.* A fluorescence polarization assay was used to generate binding affinities of HtBv and Mnv compounds to $\alpha_v\beta_3$.[41] Compound **3** and IRDye800-YC27 were used as negative controls. 5(6)-Carboxyfluorescein-cRGDfK (**cFl-cRGDfK**) was synthesized for use as a fluorescent probe against which compounds **9** or **10** (HtBv) and **5** or **6** (Mnv) compete (Figure S23). All dilutions were tested in quadruplicate.

The binding curves were fitted using nonlinear regression as above.

Molecular Modeling. All molecular modeling experiments were performed using Discovery Studio 3.1 developed by Accelrys, Inc. (San Diego, CA).

Protein and Ligand Structure Preparation. The X-ray structure of PSMA co-crystallized with the competitive inhibitor DCIBzL (PDB: 3D7H) was downloaded from the protein data bank (RCSB, http://www.rcsb.org/pdb/home/home.do).[42] The water molecules were removed while the co-crystallized ligand was used as a template to sketch **3** and **9** using the Sketch Molecules module in Discovery Studio. An $\alpha_v\beta_3$ integrin X-ray structure co-crystallized with a cyclic-RGD derivative (PDB: 1L5G) was also obtained from RCSB.[43] The water molecules were eliminated and the co-crystallized ligand was used to sketch **5** and **9**.

In Situ Ligand Minimization. Each ligand was minimized while binding to its target protein using the *in situ* ligand minimization module with the following parameters: CHARMm as an input force field, minimization algorithm as smart minimizer, maximum minimization steps equal to 1000, minimization with RMS gradient equal to 0.001 Å, and minimization energy change set equal to zero. After the minimization protocol was executed, the *in situ* minimized ligands were stripped of their nonpolar hydrogens to simplify the overall view. The protein was depicted in the form of a light gray line ribbon. The binding pocket of a protein target was surrounded with a gray sphere. The bound ligand is depicted as a stick with atoms color-coded according to element: carbon (gray), nitrogen (blue), and oxygen (red).

Preliminary in Vivo Optical Imaging and ex Vivo Biodistribution. Animal studies were undertaken in compliance with the regulations of the Johns Hopkins Animal Care and Use Committee. Male (6- to 8-week-old), non-obese diabetic (NOD)/severe-combined immunodeficient (SCID) mice (Charles River Laboratories, Wilmington, MA) were used for the current investigation and are classified into three groups, three mice in each. Group-1 was implanted subcutaneously (s.c.) with U87-MG cells at the back right flank (2.7×10^6 cells in 100 μL of 1× HBSS). Group-2 was implanted s.c. with PC3-PIP and PC3-flu cells (3×10^6 and 2.25×10^6 cells respectively each in 100 μL of 1× HBSS) at the back right and left flanks, respectively. In both group-1 and group-2, tumors were allowed to grow for 10 days before injection of the experimental agent. In both groups, mouse 1, 2, and 3 received 2 nmol, 1 nmol, and 0.5 nmol of the HtBv agent **10**, respectively. In the case of group-3, the mice were implanted s.c. with U87-MG cells at the back right flank (2.7×10^6 cells in 100 μL of 1× HBSS). U87-MG tumors were allowed to grow for 15 days before subcutaneously implanting PSMA+ PC3-PIP cells (3×10^6 cells in 100 μL of 1× HBSS) at the back left flank, and PSMA- PC3-flu cells (2.25×10^6 cells in 100 μL of 1× HBSS) at the back right leg. Group-3 mice were allowed to grow PC3-PIP and PC3-flu tumors for an additional eight days before injecting the experimental agent(s). For group-3, mouse 1 received 1 nmol of the HtBv agent **10**, mouse 2 received 1 nmol of **10** coinjected with 100 nmol of DCIBzL (to assess PSMA-binding specificity), and mouse 3 received a mixture of 1 nmol of **10** and 300 nmol of **5** (to assess $\alpha_v\beta_3$-binding specificity). For a given single injection per one mouse, all experimental agent(s) were dissolved in 100 μL of preservative-free 0.9% NaCl injection, USP as a sterile diluent and then injected intravenously (i.v.) *via* the lateral tail vein. Images were acquired after 24 h postinjection (PI) using the Pearl Imager (LI-COR Biosciences).

The Pearl Imager uses diffusive lasers optimized for IRDye800CW incorporated in the **10**. The instrument deploys a CCD camera with a field-of-view of 11.2×8.4 cm at the surface of the imaging bed. The scan time was less than 30 s for the 800 nm channel image acquisition. Images are displayed using a pseudocolor output with a corresponding scale. For all groups, images were acquired at the same parameter settings. For each group, all images were scaled to the same minimum and maximum values. Imaging bed temperature was adjusted to 37 °C. Animals were anesthetized by inhalation of isoflurane through a nose cone connected to the imaging bed. For *ex vivo* biodistribution studies of group-3, animals were sacrificed by cervical dislocation at the end of acquisition of the *in vivo* images. *Ex vivo* images were acquired by harvesting liver, spleen, gastrointestinal tract (GIT), kidneys, urinary bladder, heart, lungs, muscle, U87-MG, PC-3-PIP, and PC-3-flu tumors and displaying them on plastic Petri dishes before imaging using the same acquisition parameters implemented for the relevant *in vivo* imaging.

■ RESULTS

Chemistry. Mnv agents EUKL-DOTA **3**, cRGDfK-DOTA **5**, and cRGDfK-IRDye800 **6** were synthesized as outlined in Schemes 1 and 2. They represent the controls to which the *in vitro* binding affinities of the labeled HtBv agents could be compared. EUKL-DOTA **3** was synthesized using the reported NHS-ester **1**, which was conjugated with *N*-boc-1,4-diaminobutane followed by global deprotection and a final conjugation step with DOTA-NHS ester (Scheme 1).[22] For targeting $\alpha_v\beta_3$

**Scheme 1. Synthesis of EUKL-DOTA (3) as a Control Mnv and DOTA-Conjugated PSMA Targeting Agent**
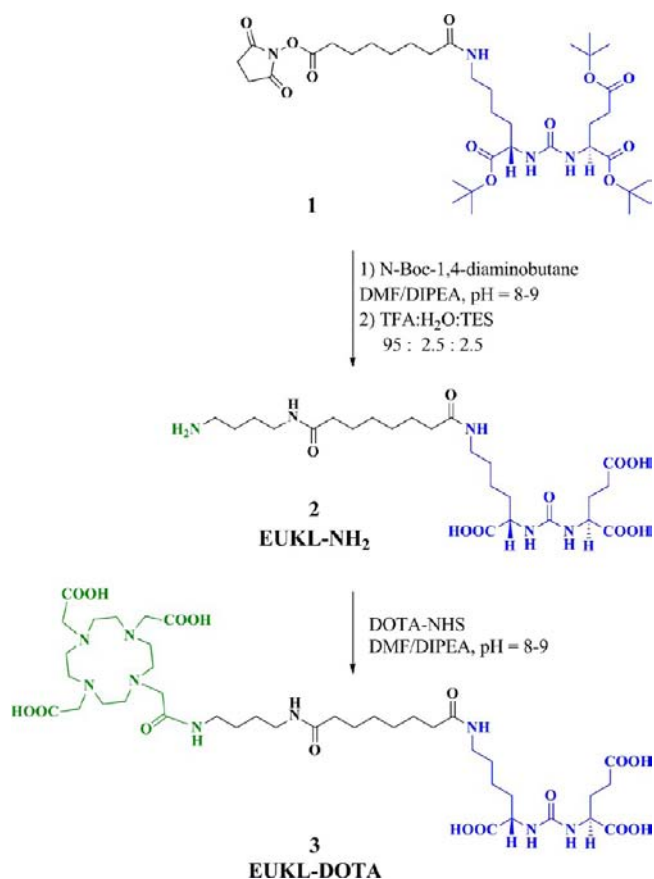
Scheme 2. Synthesis of cRGDfK-DOTA (5) and cRGDfK-IRDye800 (6) as Control and Mnv Integrin-$\alpha_v\beta_3$ Targeting Agents, Respectively
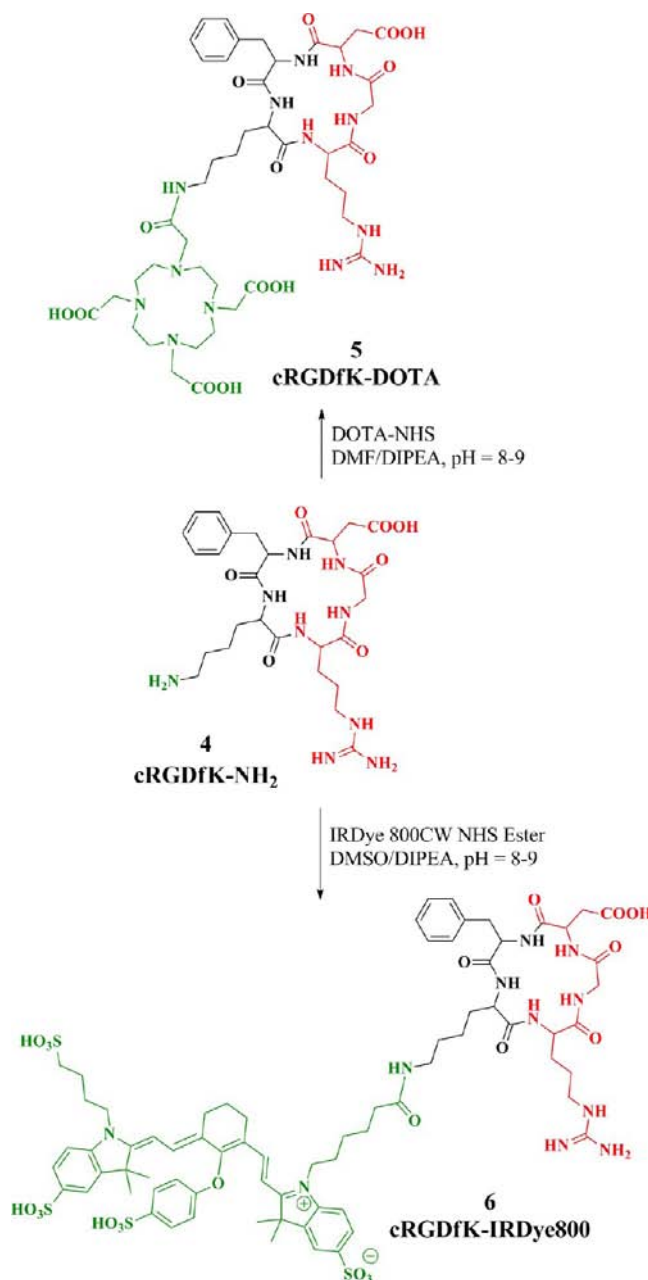
integrin, cRGDfK-NH$_2$ **4** was synthesized using a published microwave-assisted SPPS procedure.[35] Both DOTA- and IRDye800-conjugated Mnv targeted probes **5** and **6** were synthesized by reacting intermediate **4** with either DOTA-NHS or IRDye800-NHS, respectively, under appropriate conditions (Scheme 2).

Scheme 3 illustrates the synthetic route for key intermediate **8**, which can be used to generate two final, conjugated HtBv agents: DOTA-conjugated **9** or IRDye800-conjugated **10** (Scheme 4). The synthetic route of **8** began with the generation of a heterotrifunctional linker **7**, from β-glutamic acid, which can be used to assemble HtBv agents *via* conjugation with basic amine-terminated probes (pK_a < 10). Simultaneous mixing of equivalent amounts of the two amine-terminated probes with the di-NHS ester intermediate **7** proved critical to obtain the

Scheme 3. Synthesis of EUKL-cRGDfK-NH$_2$ (8)
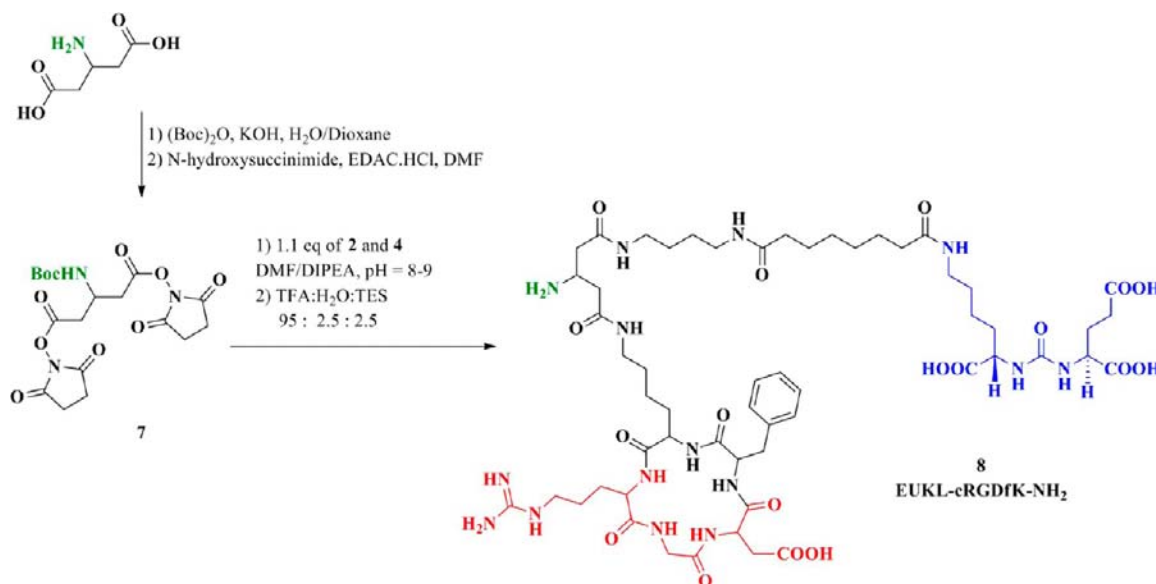
HtBv conjugate as a major product and to minimize the formation of homobivalent side products.

NIR Cell-Based Binding Affinity Measurement. The commercially available IRDye800-YC27 was used to measure the binding of DOTA-conjugated Mnv and HtBv agents to PSMA expressed by PC-3/PIP cells, while **6** was used to measure the binding of DOTA-conjugated Mnv and HtBv agents to $\alpha_v\beta_3$ integrin expressed by U87-MG cells.[21] Prior to the competitive binding experiments, the binding isotherm of each NIR agent to its target cells was constructed in order to calculate the K_d (Figure S21). As illustrated in Figure S21A, IRDye800-YC27 can saturate PSMA expressed on the surface of PC-3/PIP cells in a concentration-dependent fashion typical of specific binding, with a maximum signal of integrated fluorescence intensity equal to about 1,000. IRDye800-YC27 demonstrated a K_d of 23.8 nM, with a 95% confidence interval (95%-CI) of 23 to 26.5 nM (R^2 = 0.99). cRGDfK-IRDye800 (**6**) can saturate $\alpha_v\beta_3$ integrin expressed on the surface of U87-MG cells with a maximum signal of integrated fluorescence intensity equal to about 270 and a K_d equal to 117 nM, with a 95%-CI of 63−171 nM (R^2 = 0.92) (Figure S21B). We further validated the consistency of the PC-3/PIP cell-based assay by measuring the Z-factor (Figure S22) as a gauge of the quality of the newly developed cell-based assay (Z-factor = 0.723).[40]

To assess whether **9** retained affinity to PSMA compared to its Mnv control (**3**), a serial dilution of each compound was allowed to compete against 10 nM of IRDye800-YC27 for binding to PC-3/PIP cells. Results are graphically presented in Figure 1A and numerically described in Table 2. DCIBzL,[20] a known, high-affinity PSMA ligand, was used as a positive control. The coincidence of the 95%-CI of the IC$_{50}$ values presented by **3** and **9** indicates that the covalent linkage of cRGDfK does not significantly affect the binding of the EUKL moiety to PSMA within a cellular environment. Analogously, Figure 1C and Table 2 suggest that **9** can compete against 50 nM of **6** over binding to $\alpha_v\beta_3$ integrin on U87-MG cells, as much as Mnv **5**, which is indicated by the coincidence of the 95%-CI of the respective IC$_{50}$ values of both compounds (**5** and **9**).

PSMA Binding Assay. To confirm the results obtained by the NIR intact cell-based competitive binding assay measuring
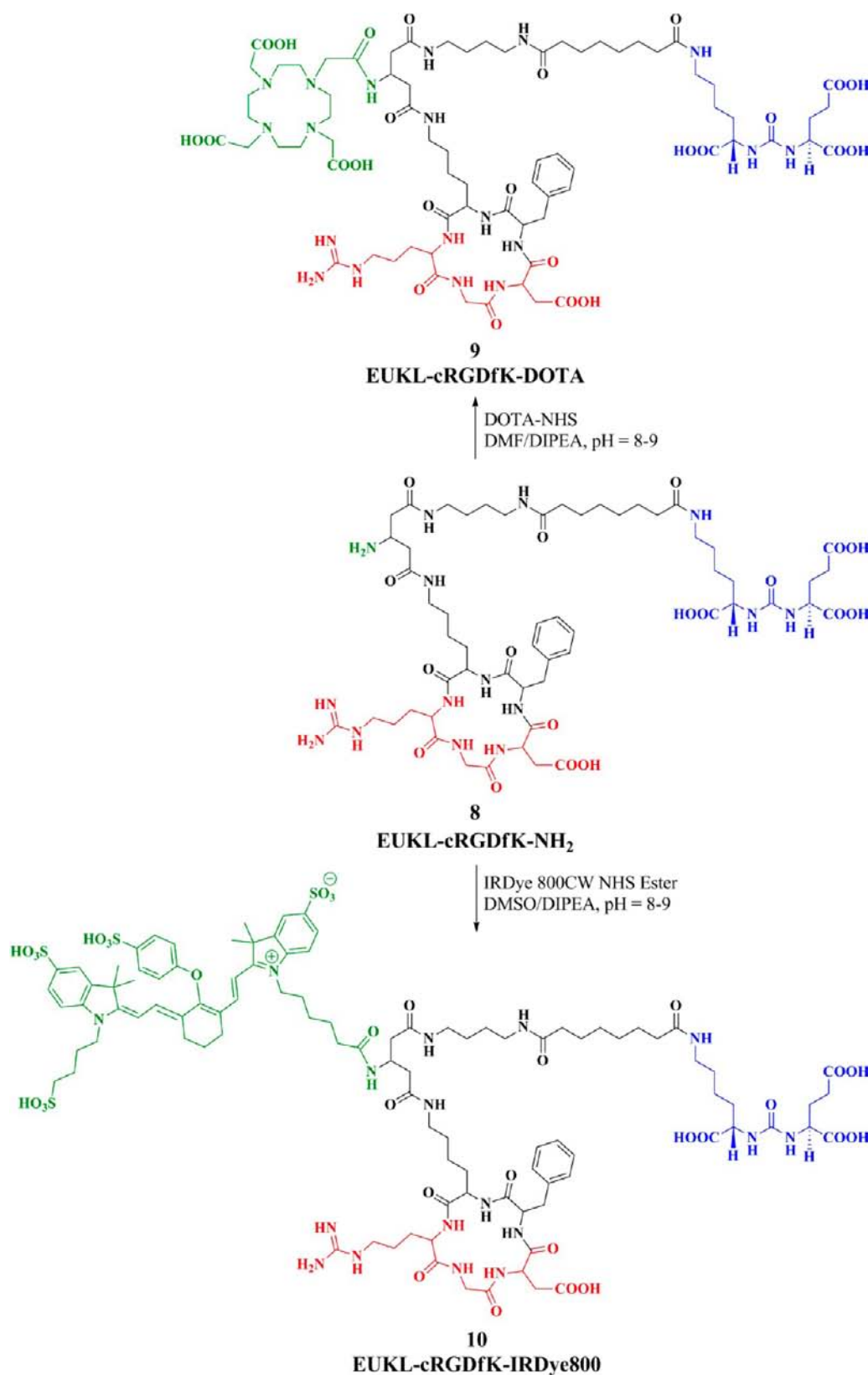
the affinities of **3** and **9** toward PSMA overexpressed on PC-3/PIP cells, a fluorescent protein-based assay was performed.[20] The IC$_{50}$ values obtained for the Mnv and the HtBv compounds (Table 2 and Figure 1B) were similar, and their 95%-CI coincide. This finding indicates that the covalent linking of the cRGDfK moiety does not affect the affinity of the HtBv compound to PSMA, as long as the urea-based scaffold is efficiently delivered to the deep PSMA binding site using a linker of suitable length.[44] The order of magnitude difference in the IC$_{50}$ values obtained from protein-based vs cell-based assay results from the difference in processes measured, namely, the ability of the test compound to inhibit the hydrolysis of N-acetylaspartylglutamic acid (NAAG) (K_m = 1.15 μM) in the amplex red assay vs its displacement of IRDye800-YC27 (K_d = 24 nM) *in cellulo*.[45]

$\alpha_v\beta_3$ Integrin Binding Assay. More accurate measurement of the affinity of several control and test compounds toward binding $\alpha_v\beta_3$ integrin was needed *in lieu* of the weak correlation between the obtained and fitted data of the NIR cell-based testing attempted for U87-MG cells (R^2 = 0.67 for **9**, Table 2). For that purpose a fluorescence polarization assay was employed.[41] The results of screening six compounds using this method are included in Table 2, illustrated in Figure 1D. Compound **3** and IRDye800-YC27 were screened as negative controls, and neither bound to $\alpha_v\beta_3$ integrin in this assay. On the other hand, HtBv compounds **9** and **10** showed similar competitive binding behavior to that exhibited by their respective Mnv controls, **5** and **6**. The obtained results support the conclusion that the incorporation of the EUKL moiety along with cRGDfK using a short linker does not alter the binding of the latter to $\alpha_v\beta_3$ integrin significantly. This fluorescence polarization assay is compatible with screening IRDye800-conjugated compounds because the measurement of the fluorescence polarization of cFl-cRGDfK, using excitation at 492 nm and emission at 519 nm, exhibits no interference by the optical properties of IRDye800 in the NIR region.[41,46]

Prediction of the Binding Mode of 9 to Its Individual Targets. In an attempt to visualize how **9** is capable of recognizing both targets without decreasing binding affinity to either PSMA or $\alpha_v\beta_3$ integrin, a series of *in situ* ligand minimization experiments were conducted using Discovery

Scheme 4. Synthesis of EUKL-cRGDfK-DOTA (9) and EUKL-cRGDfK-IRDye800 (10) as HtBv PSMA and Integrin-$\alpha_v\beta_3$ Targeting Agents

9
EUKL-cRGDfK-DOTA

DOTA-NHS
DMF/DIPEA, pH = 8–9

8
EUKL-cRGDfK-NH$_2$

IRDye 800CW NHS Ester
DMSO/DIPEA, pH = 8–9

10
EUKL-cRGDfK-IRDye800

Studio. This algorithm minimizes the agent built within the binding domain of a given protein structure. Figure 2 shows the results of two individual minimization experiments in which either **3** or **9** was subjected to the minimization procedure using a reported PSMA X-ray crystal structure, 3D7H.[42] The linker is predicted to deliver either the DOTA moiety in **3** (Figure 2A), or
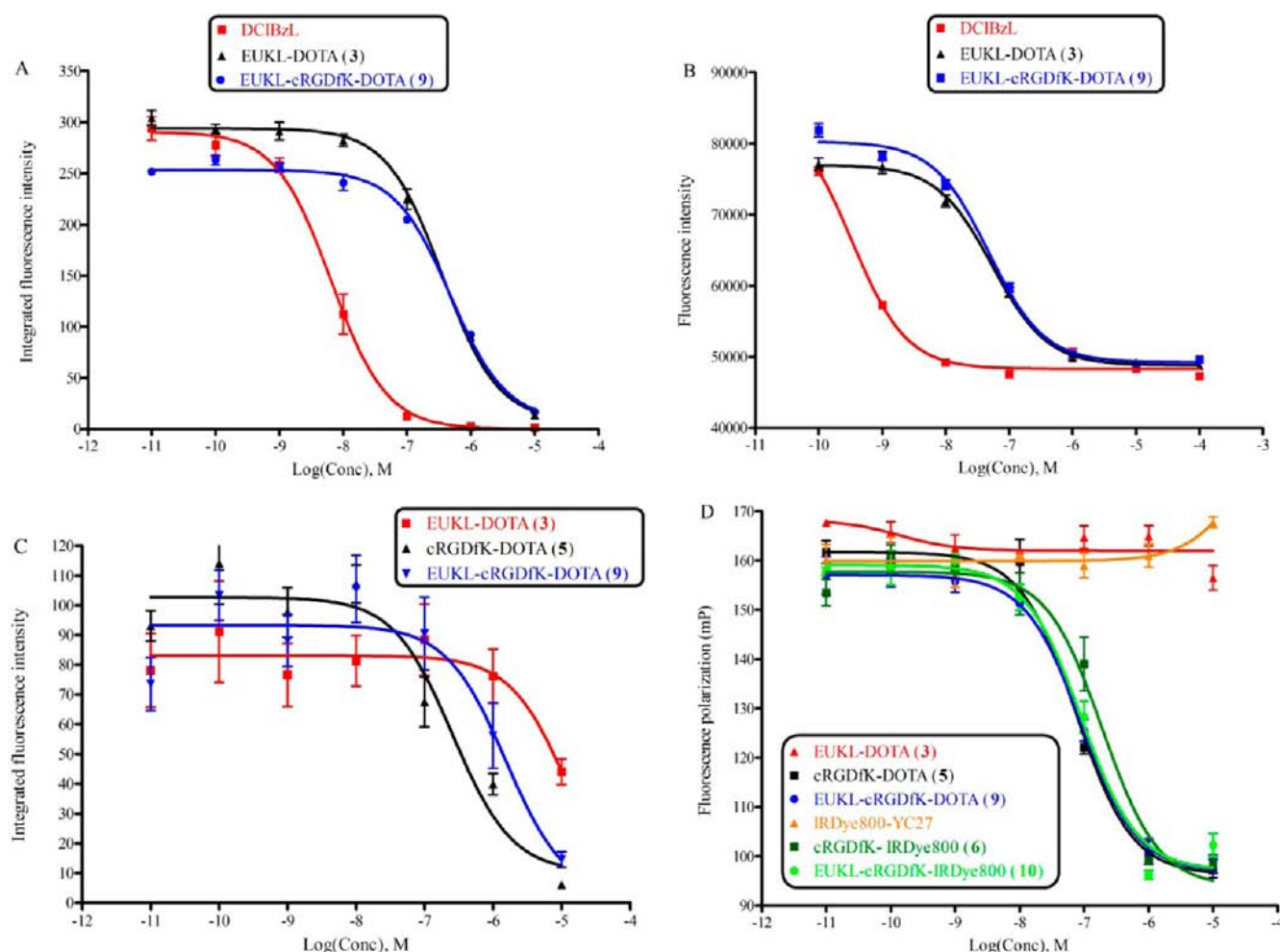
Figure 1. Competitive binding assays of test HtBv agents and their Mnv control agents. (A) NIR cell-based competitive binding to PSMA+ PC-3/PIP cells conducted against 10 nM of IRDye800-YC27. (B) Amplex red fluorescence assay (functional inhibition of PSMA). (C) NIR cell-based competitive binding to U87 cells performed against 50 nM of cRGDfK-IRDye800 (**6**). (D) Integrin-$\alpha_v\beta_3$ protein-based fluorescence polarization assay.

Table 2. [a]

| target protein	PSMA						Integrin-$\alpha_v\beta_3$					
level	Cell-based[b]			Amplex red assay[c]			Cell-based[d]			Protein-based[e]		
Compound	IC$_{50}$	95%-CI	R^2	IC$_{50}$	95%-CI	R^2	IC$_{50}$	95%-CI	R^2	IC$_{50}$	95%-CI	R^2
DCIBzL	6	4.7−8.8	0.98	0.3	0.24−0.45	0.98	ND					
EUKL-DOTA (**3**)	357	275−463	0.98	54	43−67	0.99	>10000		ND	>10000		ND
cRGDfK-DOTA (**5**)	ND						258	96−690	0.83	74	51−111	0.97
IRDye800-YC27	ND						ND			>10000		ND
cRGDfK-IRDye800 (**6**)	ND						ND			192	113−330	0.94
EUKL-cRGDfK-DOTA (**9**)	479	384−598	0.99	47	38−60	0.99	1536	383−6161	0.67	90	63−129	0.97
EUKL-cRGDfK-IRDye800 (**10**)	ND						ND			90	60−136	0.96

[a]Competitive binding assay data for HtBv agents and their Mnv control agents to both PSMA and Integrin-$\alpha_v\beta_3$. IC$_{50}$ values and 95% confidence intervals (95%-CI) are provided (nM). The goodness of the nonlinear regression fit is presented by R^2 values. ND = Not Determined. [b]NIR cell-based competitive binding over PC-3/PIP cells conducted against 10 nM of IRDye800-YC27. [c]Amplex red assay (functional inhibition of PSMA) is a fluorescence assay. [d]NIR cell-based competitive binding over human glioblastoma U87-MG cells conducted against 50 nM of cRGDfK-IRDye800 (**6**). [e]Competitive binding inhibition assay of integrin-$\alpha_v\beta_3$ protein-based fluorescence polarization assay.

the β-glutamic acid linker carrying both the DOTA and cRGDfK moieties in **9** (Figure 2B), to the space just outside of the active site of PSMA while at the same time satisfying the binding requirement between the urea and the zinc within the binding site. Figure 2C shows the Mnv and the HtBv probes superimposed upon one another, further depicting the tolerance

of **9** to addition of bulky cRGDfK and DOTA, since these latter two moieties lie outside of PSMA entirely.

The binding site of cRGDfK peptide, which is within the interface between the α_v and β_3 subunits, presents sufficient space for the accommodation of HtBv probes.[14] This space between the two subunits may explain why the inclusion of both the EUKL and/or the DOTA does not impair the binding of the
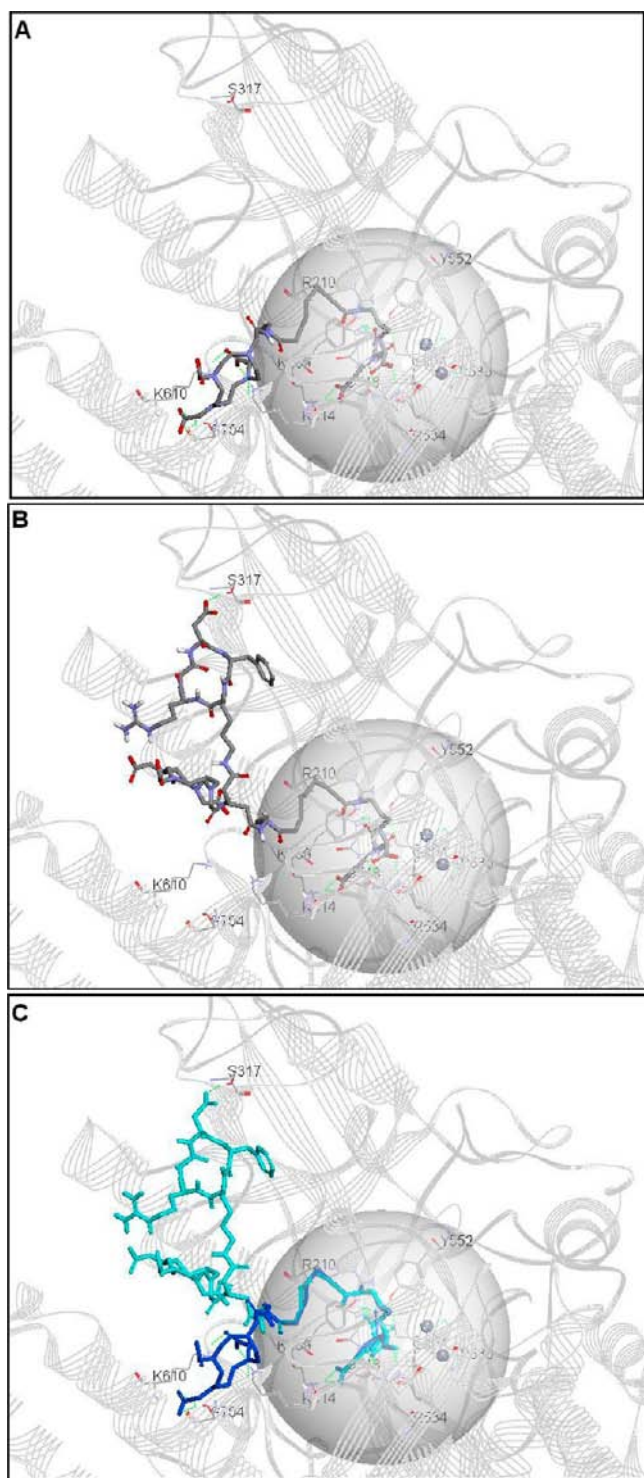
Figure 2. Proposed binding modes of compounds **3** and **9** to PSMA using an *in situ* ligand minimization protocol (Discovery Studio 3.1 client). The *in situ* experiments used 3D7H X-ray coordinates of PSMA. The protein is presented as light gray line ribbon. The binding pocket of PSMA is surrounded by a gray sphere. The bound ligand is depicted as sticks, and atoms are colored by elements in A and B; carbon (gray), nitrogen (blue), and oxygen (red). (A) Proposed binding mode of EUKL-DOTA (**3**). (B) Proposed binding mode of EUKL-cRGDfK-DOTA (**9**). (C) Superimposed compound **3** (blue) and compound **9** (cyan).

cRGDfK moiety to $\alpha_v\beta_3$ integrin. This is manifested visually in Figure 3. Compound **9** projects the PSMA targeting moiety away from the $\alpha_v\beta_3$ integrin surface (Figure 3**B**).

Preliminary *in Vivo* Optical Imaging and *ex Vivo* Biodistribution of 10. After evaluating the ability of **9** to bind to its targets (Figure 1) *in vitro*, a pilot *in vivo* study was necessary to test the ability of the HtBv probe to be useful for delivering imaging agents to tumors that may express different levels of PSMA and/or $\alpha_v\beta_3$ integrin. Compound **10** was tested for selective uptake by PSMA+ PC3-PIP, PSMA- PC3-flu, and $\alpha_v\beta_3$ integrin-expressing U87-MG cells subcutaneously transplanted in mice. Figure 4 shows the direct relationship between the tumor uptake and the injected dose of **10** in two different xenograft models: group-1 mice transplanted with U87-MG tumor and group-2 mice transplanted with PC3-PIP and PC3-flu tumors. In order to test the specificity of the uptake of **10** by either PC3-PIP tumor (PSMA mediated) or U87-MG tumor ($\alpha_v\beta_3$ integrin mediated), a blockade experiment was performed after developing an *in vivo* system that harbors all three tumor types concurrently (group-3). A mouse injected with **10** without blocking agent showed strong uptake in both PC3-PIP and U87-MG but not in PC3-flu tumor (Figure 5 A1 and B1). Blockade with 100 nM DCIBzL (a selective PSMA ligand) or with 300 nM of **5** (a Mnv, integrin-$\alpha_v\beta_3$-targeted agent) significantly reduced the uptake of **10** by PC3-PIP (Figure 5 A2 and B2) or by U87-MG (Figure 5 A3 and B3), respectively. These data suggest that **10** exhibits blockable uptake within both PC3-PIP and U87-MG tumors indicating binding specificity to each type of tumor.

■ DISCUSSION

Heteromultivalency provides agents that bind to more than one individual target, perhaps concurrently,[12] but also independently, as long as one affinity moiety does not interfere with binding of the other to its corresponding target. Multivalency and particularly heteromultivalency attempts to unite at least two separate targeting moieties that will not only be additive but may synergize either by allowing increased avidity to the overall cellular or tissue target or by enabling a statistically greater likelihood of interaction with the overall target. A multivalent agent may be needed in the context of cancer imaging or therapy, for example, in which a tumor may alter its phenotype midway through therapy, losing one target while preserving the other. Excellent reviews on multivalency exist.[47−49] Here we report the synthesis and evaluation of an HtBv ligand targeting PSMA and $\alpha_v\beta_3$ integrin, two targets expressed in certain, specific types of tumor epithelium, but also broadly on most solid tumor neovasculature, where such a HtBv agent may find useful clinical application.

In contrast to homomultivalency, in which multiple copies of the same probe, aiming at a single target, are covalently linked together to increase the overall avidity toward the target cell, heteromultivalency, targeting two different surface proteins, may or may not aim at increasing the avidity. Avidity, the affinity of a multivalent agent, can be enhanced by receptor clustering or through increased local concentration of the HtBv agent in the proximity of cells expressing one or more of the intended targets.[48,50]

Despite the fact that both PSMA and $\alpha_v\beta_3$ are localized to the cell surface, the location of the binding site in each case is different, necessitating a different strategy for covalently linking the two targeting moieties. Targeting $\alpha_v\beta_3$ by cRGDfK can be achieved superficially at the interface between the α_v and the β_3 subunits and requires a linker to the imaging moiety to be no
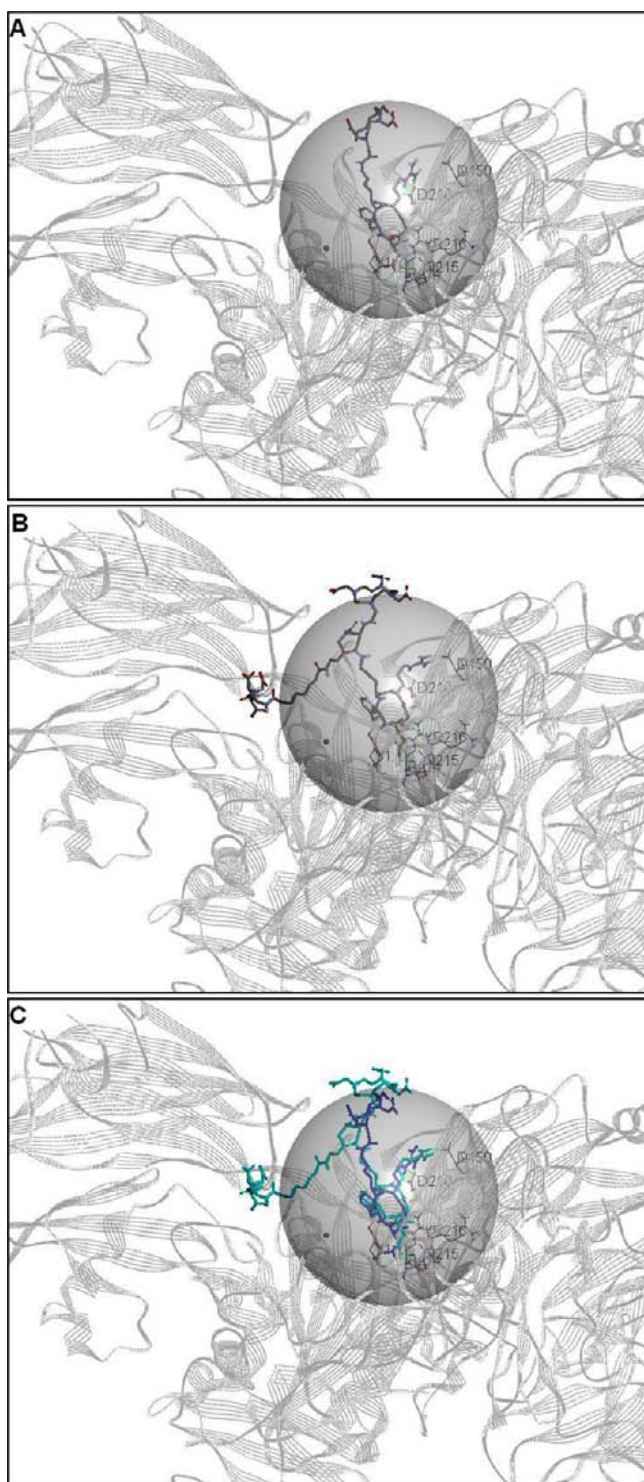
Figure 3. Proposed binding modes of compounds **5** and **9** to integrin-$\alpha_v\beta_3$ using an *in situ* ligand minimization protocol (Discovery Studio 3.1 client). The *in situ* experiments used 1L5G X-ray coordinates of integrin-$\alpha_v\beta_3$. The protein is presented as light gray line ribbon. The binding pocket of integrin-$\alpha_v\beta_3$ is surrounded with a gray sphere. The bound ligand is depicted as stick and atoms are colored by elements in A and B; carbon (gray), nitrogen (blue), and oxygen (red). (A) Proposed binding mode of cRGDfK-DOTA (**5**). (B) Proposed binding mode of EUKL-cRGDfK-DOTA (**9**). (C) Superimposed compound **5** (blue) and compound **9** (cyan).

longer than the side chain of lysine.[43] On the other side, the urea binding site lies deep within PSMA and requires a linker of approximately 20 Å in length to deliver the binding urea-based scaffold to its cognate site.[44] It is important to stress that the aforementioned 20 Å linker was implemented in the current work with the intention to deliver the PSMA targeting urea to the binding site deep within PSMA rather than allowing the HtBv agent to bind simultaneously to both PSMA and $\alpha_v\beta_3$.

For the purpose of covalently linking both EUKL and cRGDfK, a linker that offers three points of attachment is needed: one point for each targeting moiety and the third to attach an imaging moiety or other construct such as a nanoparticle, toxic species, or other. β-Glutamic acid can offer the above possibilities. Two carboxylic acid groups can be converted into NHS esters while the amino group is orthogonally protected.

In construction of an HtBv ligand the covalent modification by which two targeting moieties are linked should have a minimal effect on the binding of each moiety to its respective target. We took a graded approach by evaluating binding first *in cellulo* using an equilibrium saturation analysis for targeting PSMA. Concerning $\alpha_v\beta_3$, a radiometric cell-based assay has been widely used in measuring the affinity of $\alpha_v\beta_3$ targeting probes on a cellular level using U87-MG glioblastoma cells known to express $\alpha_v\beta_3$.[14,39] The results obtained and depicted by Figure 1A,C indicate that **9** is able to recognize both PSMA and $\alpha_v\beta_3$ *in cellulo*. As shown in Table 2, the coincidence of 95%-CI of the IC_{50} values computed for **9** and its respective Mnv control further supports the last notion. Different accuracy of the nonlinear regression fit of the competitive blockade for the PC3-PIP (PSMA) system versus the U87-MG ($\alpha_v\beta_3$) system, as indicated by the R^2 of the IC_{50} values of **3** and **9** against IRDye800-YC27 (0.98 and 0.99, respectively) vs the R^2 of the IC_{50} values of **5** and **9** against **6** (0.83 and 0.67, respectively), was observed. One of the underlying reasons for this disparity could be that the two experiments were conducted using cells that were treated differently. The PC3-PIP cells have been engineered to overexpress PSMA, while the $\alpha_v\beta_3$-positive control cells, U87-MG, naturally express the target sought after—and likely at lower levels than PSMA is expressed in the transgenic line. Nevertheless, specific binding of the HtBv agent **9** to PSMA was further confirmed by a fluorescence-based functional inhibition assay, while binding of the same agent and **10** to $\alpha_v\beta_3$ was confirmed by a cell-free, protein-based fluorescence polarization assay (Table 2).

In both cases, *in situ* ligand minimization experiments show that the second targeting moiety protrudes outside of the protein target into the surrounding aqueous environment. Both EUKL and cRGDfK moieties exhibit high water solubility, minimizing the enthalpic consequences of their association with that environment. Additionally, the short β-glutamic acid linker minimizes the entropic cost that would be conferred by a longer linker. Pilot *in vivo* optical imaging of the dose-uptake relationship (Figure 4) of compound **10** by different xenograft models expressing either target protein supports the *in vitro* results (Figure 1). Selective blockade of the PC3-PIP tumor uptake of **10** by cotreatment with an excess of the known PSMA ligand DCIBzL, and of U87-MG tumor uptake of **10** by a c-RGDfK carrier (**5**), as illustrated by Figure 5, further supports the dual targeting capacity of **10** with specificity.

■ CONCLUSIONS

PSMA and integrin-$\alpha_v\beta_3$ are overexpressed in primary tumors, neovasculature, and metastatic lesions, suggesting that they may be used concurrently as a more powerful mechanism by which to
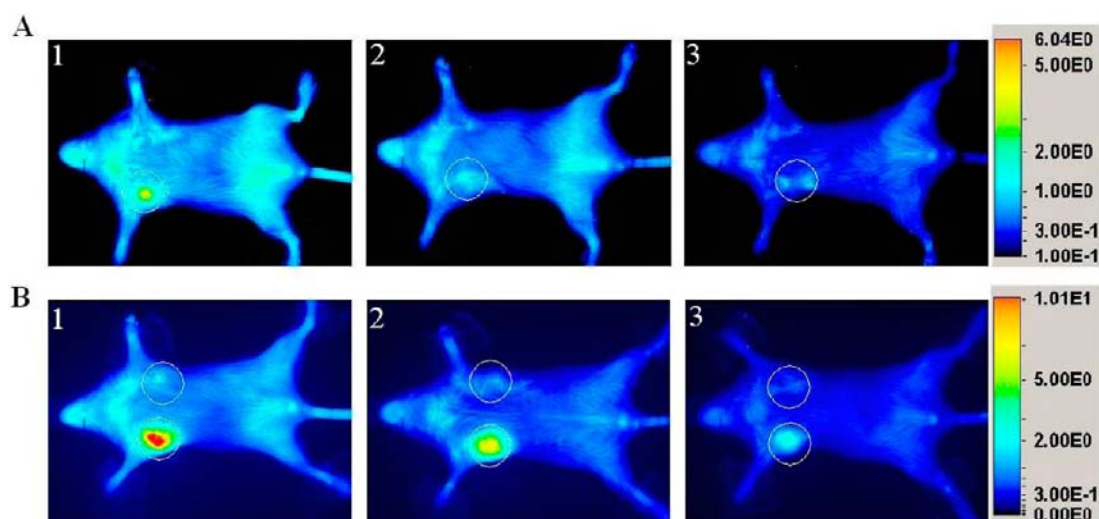
Figure 4. Dose-dependent uptake of compound **10** by two different phenotypic xenografts. (A) *In vivo* optical imaging of three NOD/SCID mice bearing U87-MG tumors (group-1 mice). Mouse 1 received 2 nmol, mouse 2 received 1 nmol, and mouse 3 received 0.5 nmol of the HtBv agent **10**. (B) *In vivo* optical imaging of three NOD/SCID mice bearing PC-3/PIP (forward left flank) and PSMA- PC-3/flu (forward right flank) tumors (group-2 mice). Mouse 1 received 2 nmol, mouse 2 received 1 nmol, and mouse 3 received 0.5 nmol of the HtBv agent **10**. Ventral (animal supine) views were obtained at 24 h postinjection. Images were scaled to the same maximum and minimum values (arbitrary units) for each group.
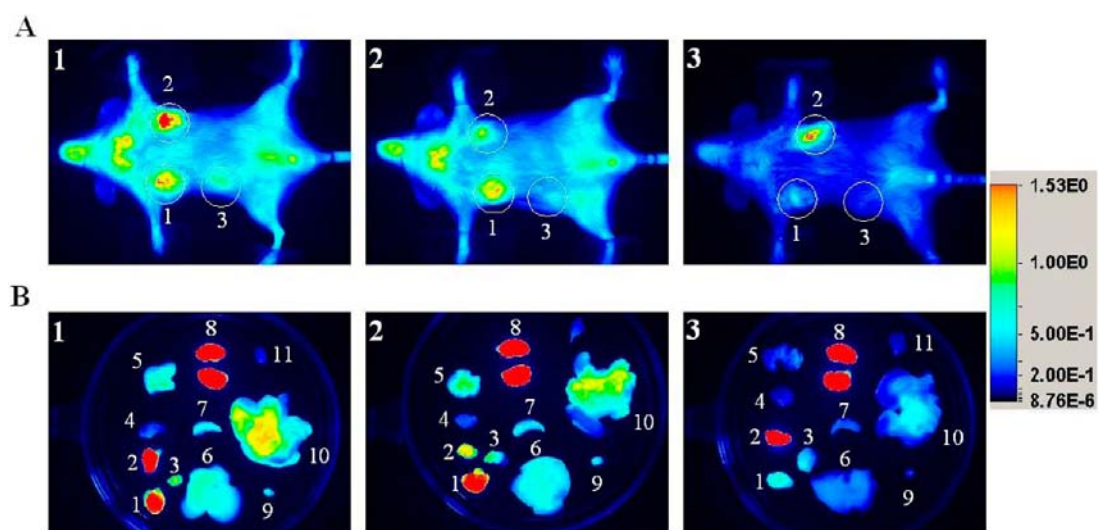
Figure 5. Binding specificity demonstrated by specific blockade of 1 nmol **10** uptake by different phenotypic xenografts using specific blockers. (A) *In vivo* optical imaging of three NOD/SCID mice bearing U87-MG (1), PSMA+ PC3-PIP (2), and PSMA- PC3-flu (3) tumors (group-3 mice). Mouse 1 received 1 nmol of the HtBv agent **10**, mouse 2 received 1 nmol of the HtBv agent **10** along with 100 nmol DCIBzL (selective PSMA ligand), and mouse 3 received a mixture of 1 nmol of the HtBv agent **10** and 300 nmol compound **5** (Mnv integrin-$\alpha_v\beta_3$ agent). Ventral (animal supine) views were obtained at 24 h postinjection. (B) *Ex vivo* Images of individually harvested organs on a Petri dish at 24 h postinjection: U87-MG (1), PC3-PIP (2), PC3-flu (3), heart (4), lung (5), liver (6), spleen (7), kidneys (8), bladder (9), GIT (10), and muscle (11). Images were scaled to the same maximum values (arbitrary units).

target imaging agents to tumors—particularly tumor-associated neovasculature. Compound **10** was capable of binding productively to each target *in vitro* and in xenograft models. *In situ* ligand minimization experiments offer an explanation of the binding data, where the EUKL and cRGDfK moieties productively occupy positions either outside the two units forming $\alpha_v\beta_2$ or PSMA, respectively. The current HtBv design in which the two targeting moieties and a radiometal chelator or an optical dye were attached *via* a short linker provides a single molecule capable of identifying two structurally and functionally different cancer-selective surface proteins. DOTA-conjugated **9** will be used for the preparation of radiolabeled derivatives for

quantitative biodistribution studies as well as additional imaging and radiotherapeutic applications in the future.

■ ASSOCIATED CONTENT

Ⓢ Supporting Information
Additional experimental details, schemes, ESI-MS spectra, and HPLC chromatograms. This material is available free of charge via the Internet at http://pubs.acs.org.

■ AUTHOR INFORMATION

Corresponding Author
*Phone: 410-955-2789. Fax: 443-817-0990. E-mail: mpomper@jhmi.edu.

■ ABBREVIATIONS

95%-CI, 95% confidence interval; ACN, acetonitrile; Boc, tertiary butoxycarbonyl; cFl-cRGDfK, 5(6)-carboxyfluorescein-cRGDfK; DIPEA, diisopropyl ethylamine; DMF, dimethylformamide; DMSO, dimethylsulfoxide; DOTA, 1,4,7,10-tetraazacyclododecane-1,4,7,10-tetraacetic acid; EDAC.HCl, 3-(ethyliminomethyleneamino)-*N,N*-dimethylpropan-1-amine hydrochloride; ESI-MS, electrospray ionization-mass spectrometry; EUKL, glutamate urea lysine linker; FBS, fetal bovine serum; HtBv, heterobivalent; GIT, gastrointestinal tract; Mnv, monovalent; NAAG, *N*-acetylaspartylglutamate; NHS, N-hydroxysuccinimide; NIR, near-infrared; Pbf, 2,2,4,6,7-pentamethyldihydrobenzofuran-5-sulfonyl; PBS, phosphate buffered saline; PET, positron emission tomography; PI, postinjection; PSMA, prostate specific membrane antigen; RP-HPLC, reverse-phase high performance liquid chromatography; SPECT, single photon emission computed tomography; SPPS, solid-phase peptide synthesis; TFA, trifluoroacetic acid; TEAA, triethylammonium acetate; TES, tetraethylsilane

■ REFERENCES

(1) Yang, S. Y., Adelstein, J., and Kassis, A. I. (2010) Putative molecular signatures for the imaging of prostate cancer. *Expert Rev. Mol. Diagn. 10,* 65−74.

(2) Mehra, N. K., Mishra, V., and Jain, N. K. (2013) Receptor-based targeting of therapeutics. *Ther. Delivery 4,* 369−94.

(3) Winnard, P. T., Jr., Pathak, A. P., Dhara, S., Cho, S. Y., Raman, V., and Pomper, M. G. (2008) Molecular imaging of metastatic potential. *J. Nucl. Med. 49* (Suppl 2), 96S−112S.

(4) Barrett, J. A., Coleman, R. E., Goldsmith, S. J., Vallabhajosula, S., Petry, N. A., Cho, S., Armor, T., Stubbs, J. B., Maresca, K. P., Stabin, M. G., Joyal, J. L., Eckelman, W. C., and Babich, J. W. (2013) First-in-man evaluation of 2 high-affinity PSMA-avid small molecules for imaging prostate cancer. *J. Nucl. Med. 54,* 380−7.

(5) Cho, S. Y., Gage, K. L., Mease, R. C., Senthamizhchelvan, S., Holt, D. P., Jeffrey-Kwanisai, A., Endres, C. J., Dannals, R. F., Sgouros, G., Lodge, M., Eisenberger, M. A., Rodriguez, R., Carducci, M. A., Rojas, C., Slusher, B. S., Kozikowski, A. P., and Pomper, M. G. (2012) Biodistribution, tumor detection, and radiation dosimetry of 18F-DCFBC, a low-molecular-weight inhibitor of prostate-specific membrane antigen, in patients with metastatic prostate cancer. *J. Nucl. Med. 53,* 1883−91.

(6) Miyamoto, D. T., Lee, R. J., Stott, S. L., Ting, D. T., Wittner, B. S., Ulman, M., Smas, M. E., Lord, J. B., Brannigan, B. W., Trautwein, J., Bander, N. H., Wu, C. L., Sequist, L. V., Smith, M. R., Ramaswamy, S., Toner, M., Maheswaran, S., and Haber, D. A. (2012) Androgen receptor signaling in circulating tumor cells as a marker of hormonally responsive prostate cancer. *Cancer Discovery 2,* 995−1003.

(7) Taylor, R. M., Severns, V., Brown, D. C., Bisoffi, M., and Sillerud, L. O. (2012) Prostate cancer targeting motifs: expression of alphanu beta3, neurotensin receptor 1, prostate specific membrane antigen, and prostate stem cell antigen in human prostate cancer cell lines and xenografts. *Prostate 72,* 523−32.

(8) Wei, D., Jiang, X., Zhou, L., Chen, J., Chen, Z., He, C., Yang, K., Liu, Y., Pei, J., and Lai, L. (2008) Discovery of multitarget inhibitors by combining molecular docking with common pharmacophore matching. *J. Med. Chem. 51,* 7882−8.

(9) Koutsoukas, A., Simms, B., Kirchmair, J., Bond, P. J., Whitmore, A. V., Zimmer, S., Young, M. P., Jenkins, J. L., Glick, M., Glen, R. C., and Bender, A. (2011) From in silico target prediction to multi-target drug design: current databases, methods and applications. *J Proteomics 74,* 2554−74.

(10) Speck-Planche, A., Kleandrova, V. V., Luan, F., and Cordeiro, M. N. (2011) Multi-target drug discovery in anti-cancer therapy: fragment-based approach toward the design of potent and versatile anti-prostate cancer agents. *Bioorg. Med. Chem. 19,* 6239−44.

(11) Roth, B. L., Sheffler, D. J., and Kroeze, W. K. (2004) Magic shotguns versus magic bullets: selectively non-selective drugs for mood disorders and schizophrenia. *Nat. Rev. Drug Discovery 3,* 353−9.

(12) Josan, J. S., Handl, H. L., Sankaranarayanan, R., Xu, L., Lynch, R. M., Vagner, J., Mash, E. A., Hruby, V. J., and Gillies, R. J. (2011) Cell-specific targeting by heterobivalent ligands. *Bioconjugate Chem. 22,* 1270−8.

(13) Xu, L., Josan, J. S., Vagner, J., Caplan, M. R., Hruby, V. J., Mash, E. A., Lynch, R. M., Morse, D. L., and Gillies, R. J. (2012) Heterobivalent ligands target cell-surface receptor combinations in vivo. *Proc. Natl. Acad. Sci. U. S. A. 109,* 21295−300.

(14) Li, Z. B., Wu, Z., Chen, K., Ryu, E. K., and Chen, X. (2008) 18F-labeled BBN-RGD heterodimer for prostate cancer imaging. *J. Nucl. Med. 49,* 453−61.

(15) Liu, Z., Niu, G., Wang, F., and Chen, X. (2009) (68)Ga-labeled NOTA-RGD-BBN peptide for dual integrin and GRPR-targeted tumor imaging. *Eur. J. Nucl. Med. Mol. Imaging 36,* 1483−94.

(16) Yan, Y., Chen, K., Yang, M., Sun, X., Liu, S., and Chen, X. (2011) A new 18F-labeled BBN-RGD peptide heterodimer with a symmetric linker for prostate cancer imaging. *Amino Acids 41,* 439−47.

(17) Bouchelouche, K., Choyke, P. L., and Capala, J. (2010) Prostate specific membrane antigen- a target for imaging and therapy with radionuclides. *Discovery Med. 9,* 55−61.

(18) Foss, C. A., Mease, R. C., Cho, S. Y., Kim, H. J., and Pomper, M. G. (2012) GCPII imaging and cancer. *Curr. Med. Chem. 19,* 1346−59.

(19) Osborne, J. R., Akhtar, N. H., Vallabhajosula, S., Anand, A., Deh, K., and Tagawa, S. T. (2013) Prostate-specific membrane antigen-based imaging. *Urologic Oncology: Seminars and Original Investigations 31,* 144−154.

(20) Chen, Y., Foss, C. A., Byun, Y., Nimmagadda, S., Pullambhatla, M., Fox, J. J., Castanares, M., Lupold, S. E., Babich, J. W., Mease, R. C., and Pomper, M. G. (2008) Radiohalogenated prostate-specific membrane antigen (PSMA)-based ureas as imaging agents for prostate cancer. *J. Med. Chem. 51,* 7933−43.

(21) Chen, Y., Dhara, S., Banerjee, S. R., Byun, Y., Pullambhatla, M., Mease, R. C., and Pomper, M. G. (2009) A low molecular weight PSMA-based fluorescent imaging agent for cancer. *Biochem. Biophys. Res. Commun. 390,* 624−9.

(22) Banerjee, S. R., Pullambhatla, M., Byun, Y., Nimmagadda, S., Foss, C. A., Green, G., Fox, J. J., Lupold, S. E., Mease, R. C., and Pomper, M. G. (2011) Sequential SPECT and optical imaging of experimental models of prostate cancer with a dual modality inhibitor of the prostate-specific membrane antigen. *Angew. Chem., Int. Ed. Engl. 50,* 9167−70.

(23) Hrkach, J., Von Hoff, D., Mukkaram Ali, M., Andrianova, E., Auer, J., Campbell, T., De Witt, D., Figa, M., Figueiredo, M., Horhota, A., Low, S., McDonnell, K., Peeke, E., Retnarajan, B., Sabnis, A., Schnipper, E., Song, J. J., Song, Y. H., Summa, J., Tompsett, D., Troiano, G., Van Geen Hoven, T., Wright, J., LoRusso, P., Kantoff, P. W., Bander, N. H., Sweeney, C., Farokhzad, O. C., Langer, R., and Zale, S. (2012) Preclinical development and clinical translation of a PSMA-targeted docetaxel nanoparticle with a differentiated pharmacological profile. *Sci. Transl. Med. 4,* 128ra39.

(24) Chang, S. S., O'Keefe, D. S., Bacich, D. J., Reuter, V. E., Heston, W. D., and Gaudin, P. B. (1999) Prostate-specific membrane antigen is produced in tumor-associated neovasculature. *Clin. Cancer Res. 5,* 2674−81.

(25) Chang, S. S., Reuter, V. E., Heston, W. D., Bander, N. H., Grauer, L. S., and Gaudin, P. B. (1999) Five different anti-prostate-specific membrane antigen (PSMA) antibodies confirm PSMA expression in tumor-associated neovasculature. *Cancer Res. 59,* 3192−8.

(26) Wernicke, A. G., Edgar, M. A., Lavi, E., Liu, H., Salerno, P., Bander, N. H., and Gutin, P. H. (2011) Prostate-specific membrane antigen as a potential novel vascular target for treatment of glioblastoma multiforme. *Arch. Pathol. Lab. Med. 135*, 1486−9.

(27) Arosio, D., Casagrande, C., and Manzoni, L. (2012) Integrin-mediated drug delivery in cancer and cardiovascular diseases with peptide-functionalized nanoparticles. *Curr. Med. Chem. 19*, 3128−51.

(28) Goodman, S. L., and Picard, M. (2012) Integrins as therapeutic targets. *Trends Pharmacol. Sci. 33*, 405−12.

(29) Goel, H. L., Li, J., Kogan, S., and Languino, L. R. (2008) Integrins in prostate cancer progression. *Endocr. Relat. Cancer 15*, 657−64.

(30) Abdollahi, A., Griggs, D. W., Zieher, H., Roth, A., Lipson, K. E., Saffrich, R., Grone, H. J., Hallahan, D. E., Reisfeld, R. A., Debus, J., Niethammer, A. G., and Huber, P. E. (2005) Inhibition of alpha(v)beta3 integrin survival signaling enhances antiangiogenic and antitumor effects of radiotherapy. *Clin. Cancer Res. 11*, 6270−9.

(31) Ye, Y., and Chen, X. (2011) Integrin targeting for tumor optical imaging. *Theranostics 1*, 102−26.

(32) Zheng, D. Q., Woodard, A. S., Fornaro, M., Tallini, G., and Languino, L. R. (1999) Prostatic carcinoma cell migration via alpha(v)beta3 integrin is modulated by a focal adhesion kinase pathway. *Cancer Res. 59*, 1655−64.

(33) Muhlhausen, U., Komljenovic, D., Bretschi, M., Leotta, K., Eisenhut, M., Semmler, W., and Bauerle, T. (2011) A novel PET tracer for the imaging of alphavbeta3 and alphavbeta5 integrins in experimental breast cancer bone metastases. *Contrast Media Mol. Imaging 6*, 413−20.

(34) Banerjee, S. R., Pullambhatla, M., Shallal, H., Lisok, A., Mease, R. C., and Pomper, M. G. (2011) A modular strategy to prepare multivalent inhibitors of prostate-specific membrane antigen (PSMA). *Oncotarget 2*, 1244−53.

(35) Yamada, K., Nagashima, I., Hachisu, M., Matsuo, I., and Shimizu, H. (2012) Efficient solid-phase synthesis of cyclic RGD peptides under controlled microwave heating. *Tetrahedron Lett. 53*, 1066−1070.

(36) Knetsch, P. A., Petrik, M., Rangger, C., Seidel, G., Pietzsch, H. J., Virgolini, I., Decristoforo, C., and Haubner, R. (2013) [(6)(8)Ga]NS-(3)-RGD and [(6)(8)Ga] Oxo-DO3A-RGD for imaging alpha(v)-beta(3) integrin expression: synthesis, evaluation, and comparison. *Nucl. Med. Biol. 40*, 65−72.

(37) Atwell, G. J., Baguley, B. C., Wilmanska, D., and Denny, W. A. (1986) Potential antitumor agents. 45. Synthesis, DNA-binding interaction, and biological activity of triacridine derivatives. *J. Med. Chem. 29*, 69−74.

(38) Cai, W., Zhang, X., Wu, Y., and Chen, X. (2006) A thiol-reactive 18F-labeling agent, N-[2-(4−18Ffluorobenzamido)ethyl]maleimide, and synthesis of RGD peptide-based tracer for PET imaging of avb3 integrin expression. *J. Nucl. Med. 47*, 1172−1180.

(39) Kumar, C. C., Nie, H., Rogers, C. P., Malkowski, M., Maxwell, E., Catino, J. J., and Armstrong, L. (1997) Biochemical characterization of the binding of echistatin to integrin alphavbeta3 receptor. *J. Pharmacol. Exp. Ther. 283*, 843−53.

(40) Zhang, J. H., Chung, T. D., and Oldenburg, K. R. (1999) A simple statistical parameter for use in evaluation and validation of high throughput screening assays. *J. Biomol. Screen 4*, 67−73.

(41) Wang, W., Wu, Q., Pasuelo, M., McMurray, J. S., and Li, C. (2005) Probing for integrin alpha v beta3 binding of RGD peptides using fluorescence polarization. *Bioconjugate Chem. 16*, 729−34.

(42) Barinka, C., Byun, Y., Dusich, C. L., Banerjee, S. R., Chen, Y., Castanares, M., Kozikowski, A. P., Mease, R. C., Pomper, M. G., and Lubkowski, J. (2008) Interactions between human glutamate carboxypeptidase II and urea-based inhibitors: structural character-ization. *J. Med. Chem. 51*, 7737−43.

(43) Xiong, J. P., Stehle, T., Zhang, R., Joachimiak, A., Frech, M., Goodman, S. L., and Arnaout, M. A. (2002) Crystal structure of the extracellular segment of integrin alpha Vbeta3 in complex with an Arg-Gly-Asp ligand. *Science 296*, 151−5.

(44) Banerjee, S. R., Foss, C. A., Castanares, M., Mease, R. C., Byun, Y., Fox, J. J., Hilton, J., Lupold, S. E., Kozikowski, A. P., and Pomper, M. G. (2008) Synthesis and evaluation of technetium-99m- and rhenium-

labeled inhibitors of the prostate-specific membrane antigen (PSMA). *J. Med. Chem. 51*, 4504−17.

(45) Mlcochova, P., Plechanovova, A., Barinka, C., Mahadevan, D., Saldanha, J. W., Rulisek, L., and Konvalinka, J. (2007) Mapping of the active site of glutamate carboxypeptidase II by site-directed mutagenesis. *FEBS J. 274*, 4731−41.

(46) Turek-Etienne, T. C., Small, E. C., Soh, S. C., Xin, T. A., Gaitonde, P. V., Barrabee, E. B., Hart, R. F., and Bryant, R. W. (2003) Evaluation of fluorescent compound interference in 4 fluorescence polarization assays: 2 kinases, 1 protease, and 1 phosphatase. *J. Biomol. Screen 8*, 176−84.

(47) Mammen, M., Choi, S.-K., and Whitesides, G. M. (1998) Polyvalent interactions in biological systems: implications for design and use of multivalent ligands and inhibitors. *Angew. Chem., Int. Ed. 37*, 2754−2794.

(48) Fischer, G., Schirrmacher, R., Wangler, B., and Wangler, C. (2013) Radiolabeled heterobivalent peptidic ligands: an approach with high future potential for in vivo imaging and therapy of malignant diseases. *ChemMedChem 8*, 883−90.

(49) Vauquelin, G., and Charlton, S. J. (2013) Exploring avidity: understanding the potential gains in functional affinity and target residence time of bivalent and heterobivalent ligands. *Br. J. Pharmacol. 168*, 1771−85.

(50) Kiessling, L. L., Gestwicki, J. E., and Strong, L. E. (2000) Synthetic multivalent ligands in the exploration of cell-surface interactions. *Curr. Opin. Chem. Biol. 4*, 696−703.